Ecological Indicators 127 (2021) 107758

Contents lists available at ScienceDirect

Ecological Indicators

journal homepage: www.elsevier.com/locate/ecolind

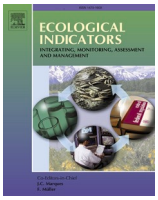

A spatial evaluation of multifunctional Ecosystem Service networks using Principal Component Analysis: A case of study in Turin, Italy

Stefano Salata [a,*], Carlo Grillenzoni [b]

[a] City and Regional Planning Department, Izmir Institute of Technology, 35430 Urla, Turkey
[b] Department of Design and Planning, Università IUAV di Venezia, 30135 Venezia, Italy

ARTICLE INFO

Keywords:
Ecosystem Services
Principal Component Analysis
Composite indicators
Overlay
Geographic information system
Environmental indicators

ABSTRACT

The multifunctional Ecosystem Service supply analysis at the spatial level is often the output of a weighted sum of layers in a Geographic Information System (GIS). This procedure is weak in detecting and representing the relationships between the input layers. Nonetheless, composite indicators produced by overlaying techniques are quite common in applied research and their discrepancies are underestimated in the scientific community, thus affecting the quality of resulting composite maps. In this work, we empirically test the effectiveness of multivariate statistics to obtain reliable composite Ecosystem Maps in the Turin metropolitan area (north-west Italy). We apply the Principal Component Analysis (PCA, using Matlab and ESRI ArcGis) to seven Ecosystem Service models (Habitat Quality, Carbon Sequestration, Water Yield, Nutrient Retention, Sediment Retention, Crop Production and Crop Pollination) and we evaluate how much the resulting composite map differs from the traditional GIS overlay. In doing this, the spectral analysis (with eigenvectors and eigenvalues) of the covariance matrix of the normalized layers confirms the heuristic arguments about the dependence between Ecosystem Services. We show that the PCA method can provide valuable results in landscape Green Network design, avoiding the limits of standard overlaying procedures. Finally, smoothing and classification techniques, applied to PCA estimates, can further improve the approach and encourage its use in various ecological indicators.

1. Introduction

The gap between the theoretical knowledge of Ecosystem Service (ES) and its implementation in plans and projects throughout the spatial representation of biophysical values might be a challenging task as it has to take into account modelling techniques (Giaimo et al., 2019a; Hansen et al., 2019; Schröter et al., 2015). In this context, an abundant number of research activities focuses on the spatial assessment of multiple ESs, while providing a synthetic representation of the overall Ecosystem Service supply (namely, Ecosystem Service Capacity - ESC) in certain areas (Baró et al., 2016; Langemeyer et al., 2016; Rosenthal et al., 2015).

ESC is generally considered a proxy of the multi-systemic land suitability here intended as the land's capacity to deliver simultaneously multiple ESs. A mathematical combination (or aggregation, as it is termed) of a set of indicators that represent the different "dimensions" of a phenomenon to be measured is called "composite index" (Alam et al., 2016; Dizdaroglu and Yigitcanlar, 2016).

In the "land suitability" theoretical debate, "good" land is the one that offers a good supporting biodiversity value (e.g. Habitat Quality) and provides several supplementary regulation benefits (e.g. Carbon Sequestration, Water Yield, Nutrient Retention and Sediment Retention), but also delivering productive capacities (e.g. Crop Production or Pollination) (Gavrilidis et al., 2017; Peccol and Movia, 2012). Although it is well-known that ESs displays synergies and trade-offs, it is generally agreed that supporting functions generates multiple benefits. On the other hand, when multiple ESs are inhibited, the land is strategically employed for anthropic-related uses (Burkhard et al., 2013; Crossman et al., 2013). ESC is then associated with a general proxy of the "quality of land", intended as the capability to provide several benefits by multiple ESs delivering capacity (Borgogno-Mondino et al., 2015; Salata, 2019).

In the Geographic Information Systems (GIS) a composite indicator is mainly produced by two different methodologies. The first approach considers ESC as the product of tabular analysis, where the composite index is the result of a statistical sum of an average qualitative index associated with a certain land use category (Raymond et al., 2017). Often, this index is reported in the bibliography and used in different contexts to assess the ES supply. This approach is quite easy to apply since it can be measured by having a land-use composition in a

* Corresponding author.
E-mail addresses: stefanosalata@iyte.edu.tr (S. Salata), carlo.grillenzoni@iuav.it (C. Grillenzoni).

https://doi.org/10.1016/j.ecolind.2021.107758
Received 1 June 2020; Received in revised form 21 April 2021; Accepted 23 April 2021
Available online 4 May 2021

Nomenclature and abbreviations

Abs	absolute
cov	covariance
CPo	Crop Pollination
CPr	Crop Production
CS	Carbon Sequestration
CV	Coefficient of Variation
det	determinant
diag	diagonal
Eq	Equation
ES	Ecosystem Service
ESC	Ecosystem Service Capacity
GIS	Geographic Information System
HQ	Habitat Quality
LLR	Local Linear regression
NR	Nutrient Retention
PCA	Principal Component Analysis
RV	Relative Variance
SAC	Spatial Autocorrelation
SD	Standard Deviation
SR	Sediment Retention
SVD	Singular Value Decomposition
var	variance
vec	vectorization
WO	Weighted Overlay
WY	Water Yield

catchment. The computation ends with a tabular weighted sum of the land uses: the final ESC is the quantity of each land use multiplied by its ecosystem capacity index.

The second approach instead considers ESC as a product of a site-specific mapping analysis produced by the spatial interaction of biophysical values in a GIS environment (Rosenthal et al., 2015; Smith et al., 2017; Van der Meulen et al., 2018). This second approach is much more relevant and difficult to apply because i) it is the product of a modelling approach employing site-specific inputs and ii) the final ESC is the product of a GIS spatial processing that complicates the procedure (Brunetta and Salata, 2019; Maes et al., 2016; Salata et al., 2017).

Measuring and evaluating the territory's environmental quality by modelling ES is a common target in environmental research. This evaluation includes various phases and is currently performed by mapping ES while inputting several layers to models (basically the Land Use Land Cover or the soil depth and characteristics, vegetation, biomass, evapotranspiration and slope) and summarizing the results in synthetic maps (Burkhard et al., 2013; Palomo et al., 2013; Salata et al., 2019). Digital cartography and GIS are necessary tools to carry out this processing. It involves both information technology and mathematical-statistics aspects, such as the utilization of procedures to practice the multivariate analysis (Graziano and Rizzi, 2016; Mubareka et al., 2011).

Many empirical studies demonstrated how the ESC utilization by mapping overlay helps reach meaningful representations of the landscape condition while supporting Green Infrastructures design and influencing decision-making (Pulighe et al., 2016; Zardo et al., 2017). However, a little attention has been devoted to analysing the interrelationship of the different ESs through GIS processing, which is often based on weighted or unweighted means of layers (Arcidiaconoet al., 2016). Particularly, a poor investigation has been devolved to see how different overlaying techniques affect the final result and, therefore, the definitive composite ESC indicator (Faisal and Shaker, 2017). Nevertheless, such an issue is crucial in understanding how standard GIS analysis can benefit from multivariate statistics when producing composite indicators.

Having experienced for many years the GIS-based ESC, the question that we want to discuss here is how to avoid certain limitations of the traditional overlaying technique, while the Principal Component Analysis (PCA) uses correlations to compress the main data into lower dimensions that retain most of the original variance.

Particularly, we want to achieve this by using the PCA to reduce strongly correlated data layers that affect the final ESC index's quality (Faisal and Shaker, 2017). As an example, if we consider a set of raster layer that comprises elevation, slope, and vegetation, there is a high probability that their spatial overlay will be "redundant", since slope and vegetation depend on elevation. Therefore, most of the variance within the study area can be explained just by the elevation.

Similarly, we are aware that while overlaying different ESs certain biophysical values has similar patterns: the Habitat Quality, the Water Yield and the Carbon Sequestration mainly depend on the Land Use Land Cover, resulting in being extremely correlated. To check how correlation influences the quality of an overall ESC index, we applied a PCA to seven raster layers produced by mapping ESs in the area of Turin (northwest Italy) and its hinterland. These layers originate from the research activity of the project LIFE Soil Administration Model 4 Community Profit (SAM4CP) (Giaimo et al., 2019a,b, Giaimo and Salata, 2019). The ES mapping activity has been conducted using the free software InVEST (Integrated Valuation of Ecosystem Services and Trade-offs), which is a suite of models used to map and value the goods and services from Natural Capital (Sharps et al., 2017; Tallis et al., 2011).

We focus our attention on the overlaying processing activity, providing a comparative analysis of two different ESC indexes, the first obtained by a traditional unweighted overlay procedure on the seven ESs. The latter employs a PCA.

We standardized the original mapping outputs regarding the unweighted overlay while summing up all layers in a final composite raster layer named "Mean" (since it represents the average value of the seven standardized inputs). Instead, the PCA process is more complex as it replaces the original layers with few output bands, which retain the same generalized variance as the original data. Raster band replacement is made by the spectral properties (eigenvectors and eigenvalues) of the covariance matrix, determining the final composition (Mubareka et al., 2011; Rodarmel and Shan, 2002).

Many statistical phases characterize the PCA: the first analyses the correlation matrix to determine the layers with a "dominant" character to the others; the second evaluates how many principal components are necessary to summarize the original ES variance. Pre-processing and post-processing phases included i) the pre-treatment of data with standardization ii) the elimination of missing values, iii) the classification and smoothing filters and iv) to the detection of spatial trends in the investigated area.

We organize the manuscript as follow: the second section introduces the methodology of research, the case study of the urban area, the mapping procedure and the two post-mapping procedures (unweighted overlay and PCA). Then, we present the results of the two methods, while in the discussion and conclusion, we compared the results of the two methodologies.

2. Methodology

2.1. Case of study (Turin metropolitan area)

Turin (Italy) is placed on the Po Fluvial Valley's western side (Fig. 1), at 240 m above sea level and near the western Italian Alpine system. It is one of the country's most populated municipalities (according to the national census, it is the fourth Italian city in terms of inhabitants):

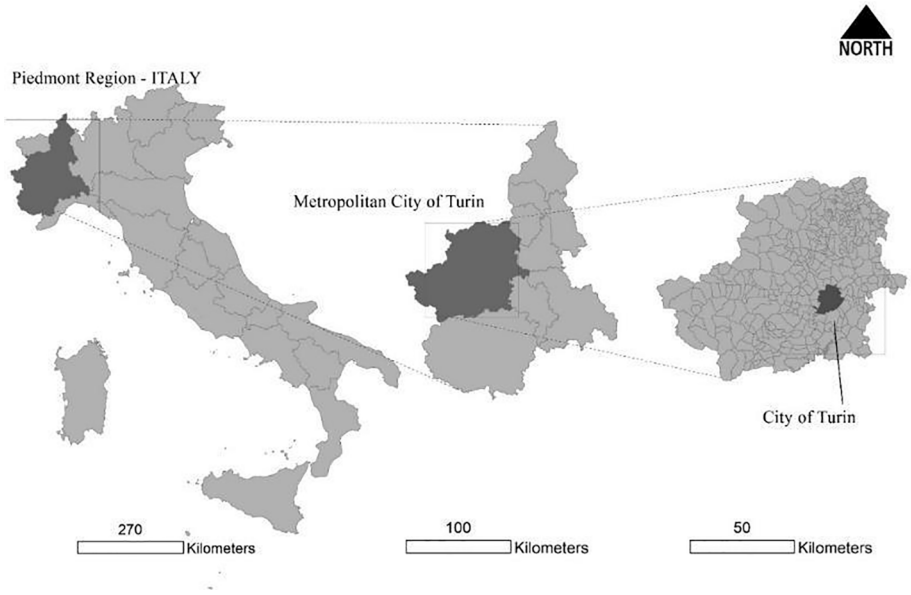

Fig. 1. The study area at various geographical scales.

about 882 thousand citizens in an administrative area of 130 square kilometres (ISTAT 2018).

The metropolitan area's morphology is heterogeneous and composed by the central city of Turin, connected by a semi-dense built-up system with scattered medium and small surrounding towns (Caldarice & Salata, 2019; Voghera & Giudice, 2019). Villages and countryside that form the sub-urban area give an urban–rural continuum composed of small natural and semi-natural patches alongside the plain valley. The agricultural land covers the most significant portion of the metropolitan area. Simultaneously, the eastern hill qualifies the city landscape and comprises a mixed anthropic settlement surrounded by a semi-natural environment.

The layer analysis has been conducted in the same unit, which included the city of Turin plus the surrounding municipalities (Moncalieri, Nichelino, Grugliasco, Pecetto Torinese, Orbassano, Settimo Torinese, San Mauro Torinese, Baldissero, Mappano, Borgaro Torinese, Collegno, Beinasco, Venaria Reale and Pino Torinese). All the considerations hereafter reported will refer to ES layers which are georeferenced by identical raster size and geographical coordinates to guarantee overlaps.

2.2. The data generation process

The European funded project SAM4CP aimed to provide a supporting decision-making model for land-use planning activities (Salata et al., 2019) by modelling the following ESs: Habitat Quality, Carbon Sequestration, Water Yield, Sediment Retention Model, Nutrient Retention Model, Crop Pollination and the Crop Production. The outputs of the model are raster layers with different pixel size modelled in the Turin metropolitan area.

- Habitat Quality (HQ). The pixel value is an index. The map recognizes the locations of the main patches of natural values. It shows the cluster where the quality of non-specific habitats (as a proxy of the overall environmental quality) is high or low.
- Carbon Sequestration (CS). Pixel value deals with tons of Carbon. The map shows the pixel's capacity to stock a different quantity of carbon while providing a "pooling" function.
- Water Yield (WY). Pixel value provides mm of water. The map represents the relative contributions of each land use cell in retaining water per watershed. The parameter of evapotranspiration has been used as an output.
- Nutrient Retention (NR). Pixel values are absolute kg nutrient. The map indicates the contribution of vegetation and soil in purifying water by removing nutrient pollutants from runoff.
- Sediment Retention (SR). Pixel values are absolute tons of soil. The map indicates the total potential soil retention per pixel in the original land cover. This information is crucial, especially in territories of a high risk of landslides (hills or mountains).
- Crop Pollination (CPo). Pixel values are pollinators. The map represents an index of the likely abundance of pollinator species on each agricultural cell in the landscape.
- Crop Production (CPr). Pixel value is the economic value of crop production per hectare. This service has been mapped using the Regional economic productivity of the different agricultural land uses.

Table 1 provides the basic descriptive statistics of the various layers, such as mean $\mu_x$and variance σ_x^2, standard deviation (SD $=$ Var$^{1/2}$), coefficient of variation (CV $=$ SD/$|$Mean$|$) and *relative variance* (RV $=$ Var/Var$_{\max}$), which is given by

$$\mathrm{RV} = \sigma_x^2 / \max_i (x_i - \mu_x)^2.$$

The CV does *not* always provide a percentage index in (0,1); hence, the actual variability of layers must be evaluated with the RV statistic. In the last column of Table 1, the layer with the greatest variability is given by CS (carbon sequestration). This does not measure the biophysical capacity but just the spatial variability (on cells of 5x5 meters) of the layer.

To make the layers homogeneous, they were divided by their maximum pixel value (rescaling 0,1 by Raster divide), where 1 indicate that an ES has been delivered at its maximum capacity. Then, we corrected the original InVEST output layers by using "filling gaps" function, and we applied the Re-sampling nearest neighbour with 1 band at 32-bit float. A map display of the 7 layers is provided in the kmz format (supplementary Google Earth) files.

2.3. Numerical overlaying techniques

Given a set of m raster layers $[\boldsymbol{X}_1, \boldsymbol{X}_2, \cdots, \boldsymbol{X}_m]$ of ecosystem services, they provide digital images of size n_1, n_2 (the number of rows, and columns). On the whole, the m layers form a *3D array* $\boldsymbol{XX}$ whose entries are x_{ijk}, with indices $i = 1, 2 \cdots n_1; j = 1, 2 \cdots n_2; k = 1, 2 \cdots m$; that is, the k-th layer of the array is given by $\boldsymbol{X}_k$ and its vectorization is $\boldsymbol{x}_k$, as in Fig. 2 below.

Table 1
Descriptive statistics of the case-study Layers (the largest values are in bold).

Layer	#Bands	Image Size	#Missing cells	Min.	Max. val.	Mean	SD	CV	RV
CPo	1	5539 × 5050	**12,370,365**	0	3.4082	1.0828	0.40156	0.3709	0.02982
CPr	1	5539 × 5055	12,370,365	0	55,292	1187.8	3381.6	2.8469	0.00391
SR	1	5541 × 5055	12,357,201	0	2342.32	12.151	44.576	**3.6686**	0.00037
NR	1	**5545 × 5056**	12,351,729	0	225.205	2.8446	8.5245	2.9968	0.00147
WY	1	5540 × 5050	12,368,263	0	439.903	235.19	84.414	0.3589	0.12882
CS	1	5539 × 5050	12,370,365	0	0.54693	0.1531	0.0900	0.5878	**0.52218**
HQ	1	5539 × 5050	12,370,365	0	1.0000	0.3227	0.2926	0.9069	0.18664

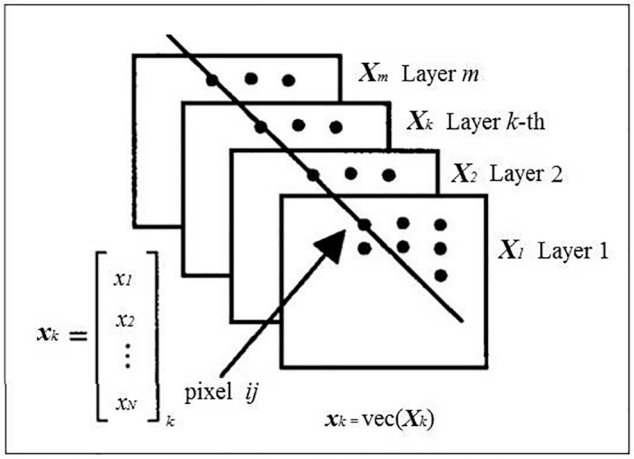

Fig. 2. Graphical representation of multi-layer GIS array (3D numerical matrix).

The fundamental goal of the multi-layer GIS analysis is to obtain a synthetic map $\boldsymbol{M}$ from the various inputs. The naive approach is to compute the simple average $\boldsymbol{M}_0 = 1/m\sum_{k=1}^{m}\boldsymbol{X}_k$; however, the result is affected by the different scale (unit of measure) of the various layers, such that those with larger range (as CPr) dominate the others. To avoid this problem, the *standardization* of each $\boldsymbol{X}_k$ requires the statistics in Eq. (1)

$$\mu_k = \frac{1}{n_1.n_2}\sum_{i=1}^{n_1}\sum_{j=1}^{n_2}x_{ijk}, \quad \sigma_k^2 = \frac{1}{n_1.n_2}\sum_{i=1}^{n_1}\sum_{j=1}^{n_2}x_{ijk}^2 - \mu_k^2, \quad k = 1,2\cdots m, \tag{1}$$

The standardization of matrices $\boldsymbol{X}_k$ is given by $(\boldsymbol{X}_k - \mu_k)/\sigma_k$, and provides the elements $(x_{ijk} - \mu_k)/\sigma_k$. A problem with this approach is that many entries become negative; hence, the simple *normalization* (division by the maximum cell value) is preferable: $\boldsymbol{X}_k^* = \boldsymbol{X}_k/\max_{ij}(x_{ijk})$. Then, the synthetic indicator is given by the average $\boldsymbol{M}^* = 1/m\sum_{k=1}^{m}\boldsymbol{X}_k^*$.

This approach is commonly implemented in GIS analysis using the Raster Overlay tool and provides consistent results to summarise different layers' information content. Its main weakness is that it does not consider the dependence between the various inputs. It follows that the matrix $\boldsymbol{M}^*$ does *not* represent the entire information content of the array $\boldsymbol{XX}$ and, therefore, may not be optimal, or objective in multiple ecosystem representation and evaluation.

2.4. Principal Component Analysis

To globally resume the m layers, the numerical techniques used in the analysis of multi-spectral remotely-sensed data may be useful. In particular, the PCA method was developed in statistics mainly for dimensional reduction reasons, i.e. to create a new array $\boldsymbol{YY}$ with a smaller number of layers, but with the same variability as the original $\boldsymbol{XX}$.

The classical PCA (Tabachnick and Fidell, 2013) is implemented on data organized in 2D matrices, which are readable by columns (the variables). In order to apply the PCA method to a 3D array, every layer $\boldsymbol{X}_k$ must be preliminary cast in vector form, obtaining the vectors$\boldsymbol{x}_k = \text{vec}(\boldsymbol{X}_k)$, of length $N = n_1.n_2$.. The resulting 2D data-matrix (equivalent to the 3D array) is then given by Eq. (2)

$$\boldsymbol{Xx} = [\boldsymbol{x}_1, \boldsymbol{x}_2 \cdots \boldsymbol{x}_m], \boldsymbol{x}_k = \text{vec}(\boldsymbol{X}_k), \tag{2}$$

with size N, m. Then, the PCA consists of obtaining a smaller 2D matrix $\boldsymbol{Yy}$, of size N, m_y, with number of columns $m_y < m$, which be nearly equivalent (in terms of variability) to $\boldsymbol{Xx}$, but having independent columns $\boldsymbol{y}_k$.Clearly, when $m_y = 1$, the matrix $\boldsymbol{Yy}$ is just a vector $\boldsymbol{y}_1$; therefore this can be reshaped in a rectangular layer $\boldsymbol{Y}_1$ of size n_1, $n_2$which summarizes all original $\boldsymbol{X}_k$.

There are various techniques to estimate the Principal Component matrix $\boldsymbol{Yy}$; the simpler one is based on the singular value decomposition (SVD) of the var-cov matrix of $\boldsymbol{Xx}$. By denoting with $\boldsymbol{x}_i^{'}$ the i-th row of $\boldsymbol{Xx}$, its mean vector $\boldsymbol{\mu}^{'}$and dispersion matrix $\Sigma_x$are given by Eq. (3)

$$\boldsymbol{\mu}^{'} = \frac{1}{N}\sum_{i=1}^{N}\boldsymbol{x}_i^{'}, \Sigma_x = \frac{1}{N}\sum_{i=1}^{N}\boldsymbol{x}_i\boldsymbol{x}_i^{'} - \boldsymbol{\mu}\boldsymbol{\mu}^{'}, \tag{3}$$

where Σ_x is square symmetrical and positive-definite of rank m. The application of the SVD technique provides the factorization $\Sigma_x = \boldsymbol{V}\Lambda\boldsymbol{V}^{'}$, where $\boldsymbol{V}$ is the orthogonal matrix of eigenvectors $\boldsymbol{v}_k$ and Λ is the diagonal (diag) matrix of eigenvalues $\lambda_k > 0$. These properties allow to define the *square root* of the covariance matrix just as $\sqrt{\Sigma_x} = \boldsymbol{V}\sqrt{\Lambda}$, wherein $\boldsymbol{V}\boldsymbol{V}^{'} = \boldsymbol{I}$ and $\sqrt{\Lambda} = \text{diag}[\sqrt{\lambda_k}]$.

The principal component transformation $\boldsymbol{Yy}$can *then* be defined by Eq. (4)

$$\boldsymbol{Yy} = \boldsymbol{Xx}\cdot\left[\sqrt{\Sigma_x}\right]^{-1} = \boldsymbol{Xx}\cdot\boldsymbol{V}^{'}\,\text{diag}\left[1/\sqrt{\lambda_k}\right], \tag{4}$$

i.e. it corresponds to a *multivariate standardization* of the original data Xx, and its components $\boldsymbol{y}_k$ become linear combinations of all vector layers $\boldsymbol{x}_k$, with weights $\boldsymbol{v}_k$. The final result of the transformation is that the columns of $\boldsymbol{Yy}$ are uncorrelated and have variances $\lambda_k > \lambda_{k+1}$, which are listed in decreasing order. These are typical statistical properties of the SVD factorization.

The main information index of the data $\boldsymbol{Xx}$ is the determinant (det) of its covariance matrix, which is called *generalized variance* (Tabachnick and Fidell, 2013). By the SVD properties, it can be shown that $\det(\Sigma_x) = \prod_{k=1}^{m}\lambda_k$, i.e. it is the product of the variances of $\boldsymbol{y}_k$; it follows that the importance of each PC in representing the data $\boldsymbol{Xx}$ is given by their eigenvalues λ_k. Since they are naturally in decreasing order, the greatest λ_1 is, concerning the others, and the better is the capacity of $\boldsymbol{y}_1$ to represent the original data $\boldsymbol{Xx}$. Usually, the necessary threshold is that $\lambda_1/\sum_{k=1}^{m}\lambda_k > 50\%$, in which case $\boldsymbol{y}_1$ provides an *effective* dimensional reduction of $\boldsymbol{Xx}$, useful for spatial mapping purposes. In general, the first component $\boldsymbol{y}_1$ is the most suitable as a synthetic indicator of the layers $\boldsymbol{X}_k$; it considers both the variability and dependence of the input layers, and by reshaping it in matrix form as $\boldsymbol{M}_1 = \text{vec}^{-1}(\boldsymbol{y}_1)$, it can be visualized as a map.

The computing process we have outlined above can be summarized in the scheme of Eq. (5)

$$(\boldsymbol{X}_k \rightarrow \boldsymbol{x}_k \rightarrow \boldsymbol{Xx}) \rightarrow \left(\Sigma_x \rightarrow \boldsymbol{V}\sqrt{\Lambda}\right) \rightarrow (\boldsymbol{Yy} \rightarrow \boldsymbol{y}_1 \rightarrow \boldsymbol{M}_1) \quad (5)$$

This is similar to the PCA of remote-sensed data (Rodarmel and Shan, 2002); however, these analyses are affected by spatial autocorrelation (SAC) between units (areas or cells). Classical PCA assumes the independence of the rows of $\boldsymbol{Xx}$, and this is obtained by random sampling; however, in temporal and spatial series, this does not hold, especially in raster data. The presence of SAC usually makes the estimates inefficient and biased, requiring a remedy. In regression analysis, the "cure" consists of introducing lagged terms among the regressors (Grillenzoni, 2004). Extending this approach to PCA, the matrix $\boldsymbol{Xx}$ must be *augmented* with the neighbors of each pixel (Switzer and Green, 1984). This means creating m additional layers $\boldsymbol{X}_{-k}$, whose entries are the average of the 8 nearest neighbors of x_{ijk}, as in Eq. (6)

$$x_{-ijk} = \frac{1}{8}\left(\sum_{r=-1}^{1}\sum_{s=-1}^{1} x_{i-r,j-s,k} - x_{ijk}\right) \quad (6)$$

Subsequently, the resulting matrices $\boldsymbol{X}_{-k}$ must be vectorized, inserted in the 2D data matrix $\boldsymbol{Xx}$ (whose number of columns double) and then tabulated in the new 2 m,2m matrix Σ_x, etc. As above mentioned, at the end of the computation only the first column $\boldsymbol{y}_1$ of the PC matrix $\boldsymbol{Yy}$ is considered and can be represented as a map that summarizes the original ecosystem layers.

A synthesis of the method discussed above is reported in Fig. 3, while a numerical example of the matrix computations is provided in Appendix A.

3. Empirical findings

The ESRI ArcGis Principal Components is an easy-to-use tool since it requires only a few inputs. Before applying it to the Turin case study, let us describe the basic steps of the diagram in Fig. 3:

1) Resize the 7 layers to the common grid 5539x5050;
2) Vectorize the layers and drop the cells with missing values, to obtain $\boldsymbol{Xx}$;
3) Normalize the columns with their maximum, and compute the mean $\boldsymbol{x}_1$;
4) Compute the covariance and correlation matrices $\Sigma_x, \mathbf{P}_x$;
5) Factorize the covariance matrix as $\Sigma_x = \boldsymbol{V}\Lambda\boldsymbol{V}'$;
6) Compute the first principal component $\boldsymbol{y}_1 = \boldsymbol{Xx}.\boldsymbol{v}_1$;
7) Reshape $\boldsymbol{x}_1, \boldsymbol{y}_1$ into 5539x5050 matrices and compare the images;
8) Classify and smooth the average layers to identify spatial patterns.

Table 2 provides the pre-processed layers' correlation matrix; the most significant values are those between HQ-CS (0.67) and CS-WY (0.72). These correlations point out the CS variable's central role, which is the component with the highest relative variance in Table 1.

The covariance matrix in Table 3 is not singular, i.e. $\det(\Sigma_x) > 0$, thus its SVD factorization runs smoothly, providing the eigenvectors and eigenvalues in Table 4. In the summary of Table 5, the first principal component $\boldsymbol{y}_1$ captures 2/3 the total variance of Σ_x; hence, it well represents the var-cov of the original layers. Further, all the weights of the first eigenvector $\boldsymbol{v}_1$ are positive, meaning that the component $\boldsymbol{y}_1$ have all positive values and provides a synthetic ES indicator. Further, computing the correlation with the initial layers $\boldsymbol{Xx}$, one can see that $\boldsymbol{y}_1$ is mainly formed by the HQ and CS components (see the last 2 columns of Table5).

Finally, by reshaping the estimated vectors $\boldsymbol{x}_1, \boldsymbol{y}_1$ (the arithmetic mean of $\boldsymbol{Xx}$ and its first principal component) in matrix form, one can obtain 5539x5050 images, which can be mapped. The results are in Fig. 4, both in grayscale (0,1) and pseudo-color (1 band, not RGB), enhancing their difference.

To evaluate the numerical differences between the two images (Mean and PCA), statistical indicators and filtering procedures must be applied. By rescaling both images in the interval (0,1), one can compare their descriptive statistics (Grillenzoni, 2008a). In Table 6 one can see that all statistics of PCA1 are significantly greater than those of the Mean; this explains the better contrast of Fig. 4b and the better ability of the PCA technique to resume the variability (information) of the 7 original layers.

Table 6. Descriptive statistics of the images in Fig. 4.

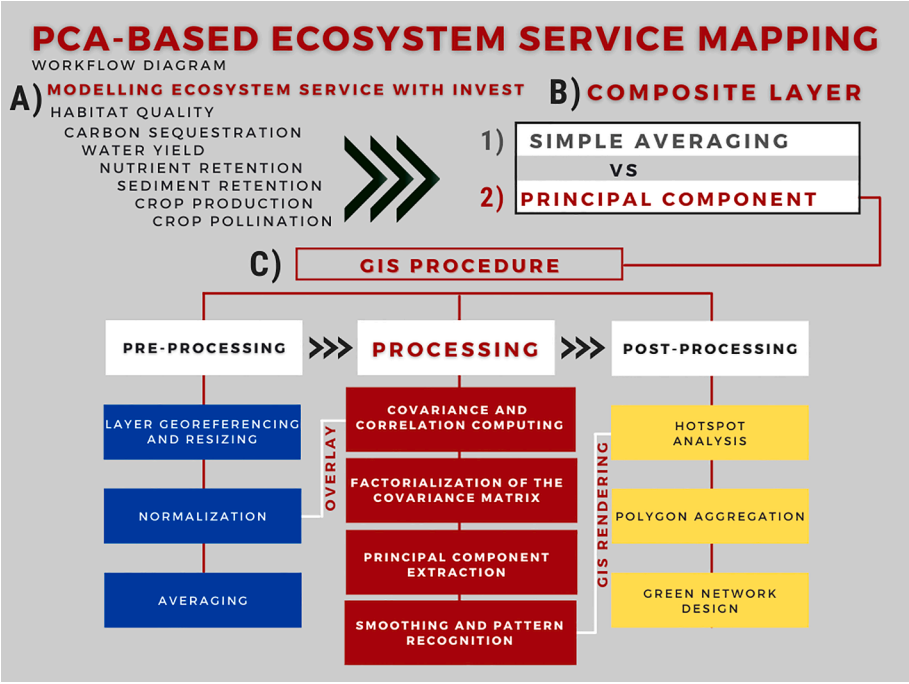

Fig. 3. Workflow diagram of the PCA-based method.

Table 2
The correlation matrix $\mathbf{P}_x$ of 7 ES layers.

Layer	HQ	CS	WY	NR	SR	CPr	CPo
HQ	1,00000	**0.6726**	0.3719	0.0953	0.2692	0.0816	0.1464
CS	**0.6726**	1,00000	**0.7239**	−0.0122	0.2597	−0.0557	0.0557
WY	0.3719	**0.7239**	1,00000	0.1530	0.0371	0.1508	0.1306
NR	0.0953	−0.0122	0.1530	1,00000	−0.0304	0.2077	−0.2669
SR	0.2692	0.2597	0.0371	−0.0304	1,00000	−0.0381	0.1739
CPr	0.0816	−0.0557	0.1508	0.2077	−0.0381	1,00000	−0.3418
CPo	0.1464	0.4914	0.1306	−0.2669	0.1739	−0.3418	1,00000

Table 3
The covariance matrix Σ_x of 7 ES layers.

Layer	HQ	CS	WY	NR	SR	CPr	CPo
HQ	0.0856	0.0324	0.0209	0.0011	0.0015	0.0015	0.0050
CS	0.0324	0.0271	0.0228	−0.0001	0.0008	−0.0006	0.0095
WY	0.0209	0.0228	0.0368	0.0011	0.0001	0.0018	0.0030
NR	0.0011	−0.0001	0.0011	0.0014	−0.0000	0.0005	−0.0012
SR	0.0015	0.0008	0.0001	−0.0000	0.0004	−0.0000	0.0004
CPr	0.0015	−0.0006	0.0018	0.0005	−0.0000	0.0037	−0.0025
CPo	0.0050	0.0095	0.0030	−0.0012	0.0004	−0.0025	0.0139

Table 4
Eigenvectors and eigenvalues of the factorization $\Sigma_x = V\Lambda V'$.

K	v_1	v_2	v_3	v_4	v_5	v_6	v_7	λ_k
1	**0.8254**	−0.5243	−0.0977	−0.0554	0.1747	0.0242	−0.0058	**0.1120**
2	**0.4226**	0.3332	0.3263	0.3021	−0.7115	−0.0619	−0.0511	**0.0330**
3	**0.3616**	0.7699	−0.3627	−0.0876	0.3645	0.0580	0.0322	**0.0166**
4	**0.0102**	0.0033	−0.1071	−0.0576	0.0208	−0.9923	−0.0066	**0.0030**
5	**0.0149**	−0.0109	0.0249	0.0104	−0.0511	−0.0108	0.9981	**0.0027**
6	**0.0127**	0.0018	−0.2370	−0.8497	−0.4661	0.0653	−0.0086	**0.0012**
7	**0.0939**	0.1455	0.8272	−0.4153	0.3318	−0.0568	0.0002	**0.0003**

Table 5
Summary of the PCA statistics.

K	λ_k	v_1	$\frac{\lambda_k}{\sum_{k=1}^{7}\lambda_k}$	$R_{xj,y1}$	X_j
1	**0.1120**	**0.8254**	**0.6632**	**0.9440**	**HQ**
2	0.0330	0.4226	0.1955	0.8596	CS
3	0.0166	0.3616	0.0984	0.6310	WY
4	0.0030	0.0102	0.0180	0.0907	NR
5	0.0027	0.0149	0.0158	0.2624	SR
6	0.0012	0.0127	0.0073	0.0698	CPr
7	0.0003	0.0939	0.0018	0.2669	CPo

$$D_{xy} = \frac{1}{n_1.n_2}\sum_{i=1}^{n_1}\sum_{j=1}^{n_2}|y_{ij} - x_{ij}|, \tag{7}$$

In particular, the first statistic shows that pixels of PCA1 are 6.6% bigger (on average) than those of the simple Mean. The analysis of the histograms is even more revealing, see Fig. 5. While the Mean image is unimodal (i.e. it has a single peak), the histogram of PCA1 is three-modal. This enables a direct segmentation of the image in 3 well-separated groups of cells: urban, *peri*-urban and hills (say) (Grillenzoni, 2016).

Fig. 6 confirms the mean technique's weakness to detect the land zones with high ES quality (in yellow color). Further, to enhance the differences and to see the spatial trends of ecological features, one can smooth an image $\boldsymbol{Y} = \{y_{ij}\}$ with nonparametric filters, as the kernel regression in Eq. (8)

$$g(i,j) = \sum_{k=1}^{n_1}\sum_{h=1}^{n_2} w_{kh}(i,j)y_{kh}, \quad w_{kh}(i,j) \propto G_a(i-k).G_b(j-h), \tag{8}$$

where the local weights $w(.)$ are proportional to the product of Gaussian (G) densities with scales $a, b > 0$. The local linear regression (LLR) smoother improves $g(i,j)$ at the borders (Grillenzoni, 2008b). Fig. 7 (produced by LLR on the images of Fig. 4) emphasizes the difference between the two methods and the better ability of PCA to detect spatial trends and clusters.

4. Analysis and discussion

4.1. Ecosystem service capacity maps based PCA method

Previous analysis has shown the better performance of PCA technique compared with the "mean" approach. The main reason is that PCA captures the relationships between inputs through the correlation matrix. Moreover, PCA explains synergies or trade-offs among ESs (Burkhard et al., 2012; Turkelboom et al., 2015).

- CS and WY have the greatest positive correlation (0.72), displaying a synergy between the two layers and their similar condition. This result can be explained by analyzing the ES input data: both depend on soil depth, soil quality, the above and below-ground biomass and vegetation;
- Even HQ and CS have a positively correlated synergy. Therefore, when the overall environmental quality is high (HQ), also the quantity of carbon stored in soil (CS) displays high values. This is evidence of the similarity of the two layers: where the landscape is suitable for hosting biodiversity it also has a good capacity to store carbon in the above and below-ground biomass. Hence, even the mean of HQ and CS can be considered "redundant" during multi-layered analysis;
- On the contrary, CPr and CPo display a trade-off pattern: when the value of CPr tends to grow, the value of CPo tends to diminish. The

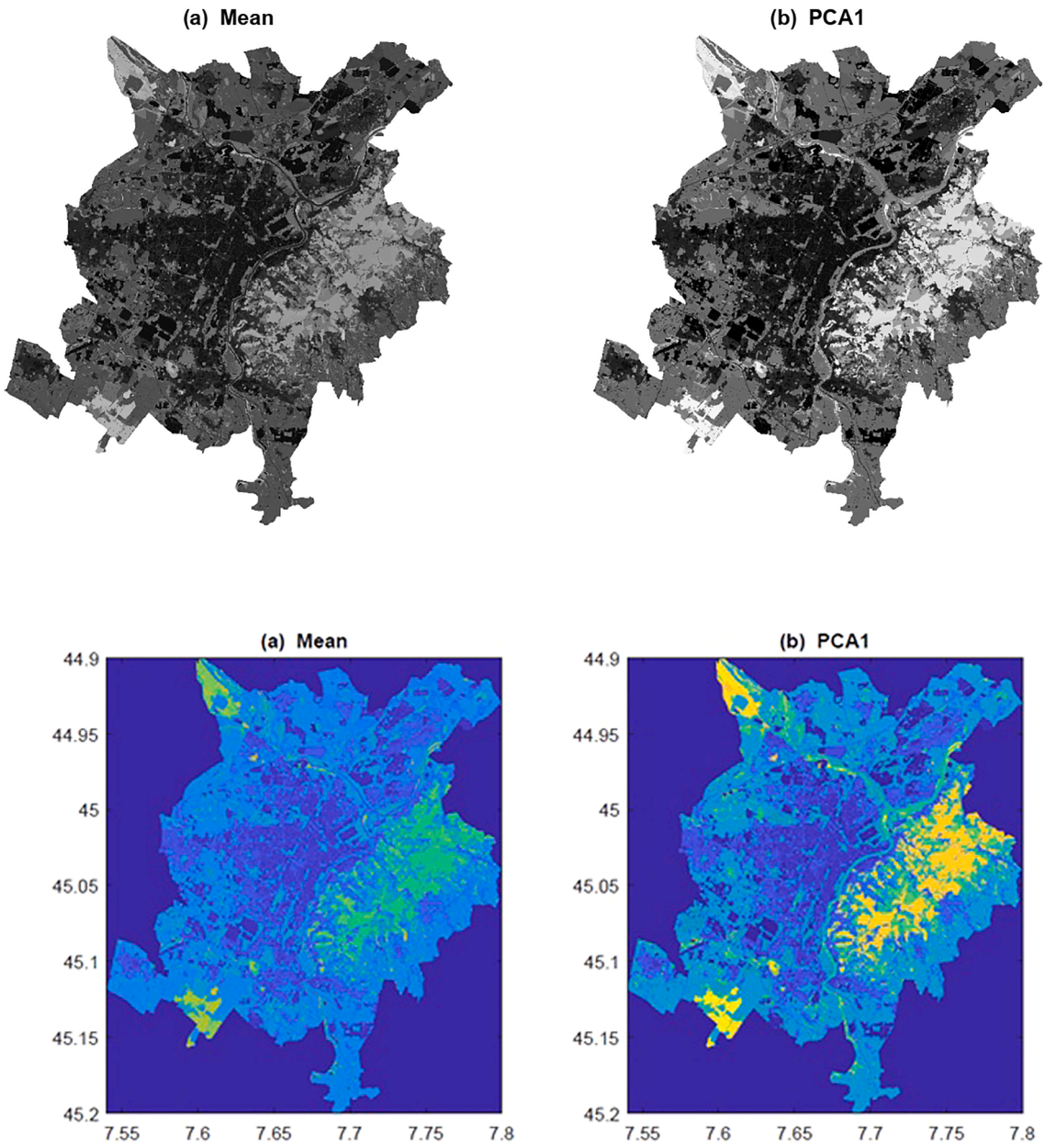

Fig. 4. Mean and PCA1 images which summarize 7 original ES layers in Grayscale (above) and Pseudo-color (below).

Table 6
also provides, in the last two columns, the mean differences between the images; the absolute one is computed in Eq. (7).

Method	Average	SD	CV	RV	Mean Diff.	Abs. Diff.
Mean	0.30087	0.16611	0.55211	0.05645		
PCA1	0.36734	0.24310	0.66152	0.14753	+0.06647	0.08293

negative correlation can be understood as a signal of the inverse relation between soil productivity and the presence of wild pollinator species. The more agricultural land's economic productivity is maximized (even employing nutrients for example in vineyards), the more pollinators are threatened. Even in negative patterns, the simple "mean" method fails to represent the correlations between the original layers.

Secondly, the correlation matrix clearly shows that CS, HQ and WY are the more synergic layers displaying a "dominant" pattern in the matrix. This result is highlighted in Table 5 (correlation between the layers $\boldsymbol{x}_j$ and the principal component y_1), where it can be noted that the PCA1 is correlated 0.94 with HQ, 0.85 with CS and 0.63 with WY. HQ, CS and WY are overall considered good proxies of a healthy environment; therefore, it is not surprising that these three layers can be regarded as "interchangeable" while describing the overall ES quality. PCA overcomes the layer redundancy while synthesizing new values in the first component. After a careful statistical and spatial analysis, 66% of the original var-cov was considered a sufficient value to extract the first component among the seven bands generated by the PCA. The final layer creates a sharpened distinction between low/high ecosystem values.

4.2. Comparison with traditional overlay

As expected, the two outputs (Mean and PCA1) agree in providing a final ESC indicator that underlines the distribution of landscapes characters in the city of Turin. Fig. 4 shows that the Corso Casale/Corso

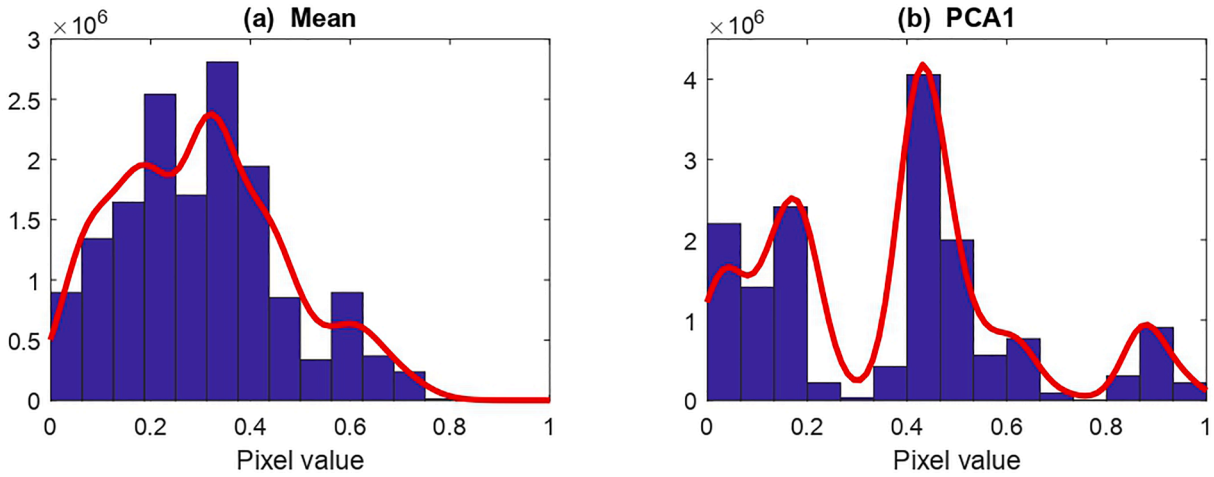

Fig. 5. Histograms of the pixel values of the Mean and PCA1 images.

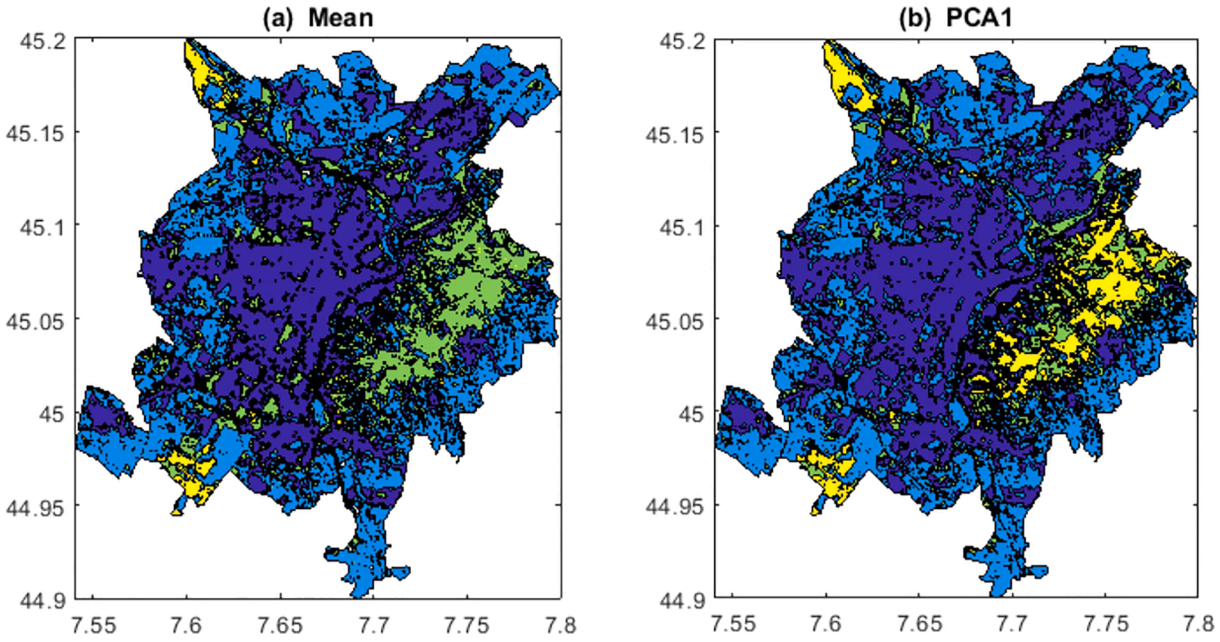

Fig. 6. Segmentation of Mean and PCA1 images in 3 classes. Notice that the third class (yellow colour, of highest ecological value) in Panel (a) is negligible. (For interpretation of the references to color in this figure legend, the reader is referred to the web version of this article.)

Moncalieri axes and their connection with the city hill bordering the Po River until Madonna del Pilone and Sassi fraction in the north and the Parco del Valentino, Borgo Pilonetto and the Sangone River confluence on the south are among the valuable urban-green corridors of Turin. But even the northern part along the Stura River displays high capability to support many ESs.

Nonetheless, as described by statistics, the visual comparison of the false pseudo colour and the smoothed version (Fig. 7) reveals some differences among the two versions: it can be noted that PCA1 is more "contrasted" and "clear", since it deletes the "background noise" that affects the Mean operator. This effect results from a diffuse redundancy of similar ES values in the unweighted overlay that contrasts with the clearer distinction between high/low values visible in Fig. 6.

PCA1 also enhances pixel clustering, especially in those dense built-up areas where the composite value of ES is much lower than the surrounding unbuilt green land. Looking at the values of both maps, the average standard deviation (SD) is significantly higher in the PCA1 (0.24310) instead of the Mean value (0.16611), revealing the capability of PCA1 to "describe" the environmental character of the catchment. Moreover, looking at the distribution of data (Fig. 5), it can be noted that while the Mean displays a uniform distribution of data, the PCA reaches three different peaks demonstrating a slightly better capacity to create an actual segmentation of values.

The higher clustering capacity of the PCA1 map is appreciated during decision-making processes (ESC map) to simplify the city's environmental quality description. Indeed, PCA1 displays a higher performance in supporting landscape planning to design areas of conservation, valorisation or compensation for future land-use changes.

4.3. ESC index to support green network design

The GIS overlay technique applied to ecological and environmental studies has demonstrated its usefulness in understanding and governing urban and landscape design (BenDor et al., 2017; McHarg, 1969).

The introduction of different Ecosystem Service digital models and maps requires a more sophisticated utilization of layers to provide synthetic and reliable representations of the overall ecosystem quality of the landscape (Lovell and Taylor, 2013; Nin et al., 2016; Young and

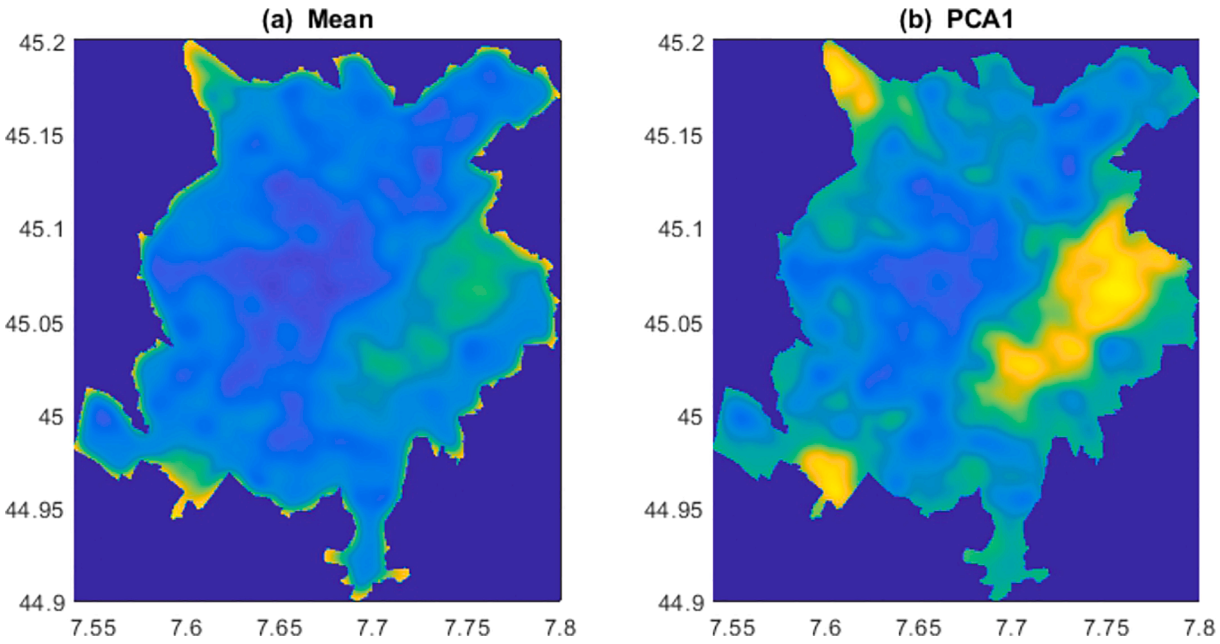

Fig. 7. Smoothed Mean and PCA1 images by mean of the local linear regression (LLR) smoother.

McPherson, 2013). This is particularly true in densely anthropic systems (Brenner, 2002; Brenner and Schmid, 2015), where the need to represent the different "internal" ecosystem gradient is relevant.

Within this background, PCA demonstrates how certain methodological innovation of the overlaying technique increased the clarity of the final output layer while emphasizing the spatial gradients and the quality of multiple ecosystems (Grêt-Regamey et al., 2017, 2015). PCA provides a sharper differentiation of "urban" ecosystems, helping to achieve a better "internal" classification of densely-populated areas.

This finding has several practical implications in environmental research since using GIS software to post-processing digital ES maps has increased during the last years. Specifically, when the final composite layer is more "contrasted", then post-process clustering to identify high/low values is more effective in designing green multifunctional urban networks. It follows that PCA output can be used as an automatic digital method to identify ecosystem clusters by employing Hotspot Analysis, and select all those multifunctional urban areas that can be grouped to define an ecosystem network.

To demonstrate the practical utilization of PCA in designing multifunctional Ecosystem Service networks, the following treatment is applied: the PCA final layer is vectorized by raster to polygon function, then the polygons are used as input for a Hotspot Analysis (with a user-defined search radius – in this case 150 m), finally the GI-Bin high values (>3) are extracted and unified by the aggregate polygons function to obtain a green multisystemic network (Salata et al., 2019).

The final result is displayed, at the urban scale (1:100,000), in Fig. 8a. It shows that the Post-processed PCA-based ESC indicator approaches the iconographic Metropolitan Green Belt of Turin designed by Cassatella (2013) in Fig. 8b, with scale (1:200,000).

This result is valuable for two main reasons:

- the final green network details the Metropolitan Green Belt of Turin while selecting and representing the continuity and contiguity between green elements inside the urban catchment. This is a fundamental requirement of well-designed urban green networks; e.g. the Stura di Lanzo River green corridor, the areas along the Dora River or the southern green *peri*-urban areas bordering the dense settlement system;
- the green network is designed using the highest ground resolution (e.g. employing the cadastral database), thus reaching an overall geometrical precision at the city-scale where ecological conservation strategies are defined.

We are aware that these empirical findings are not the product of prolonged testing of this methodology in several urban areas; rather, they are the first experimental study in a medium-size city of northern Italy. The PCA utilisation experience for ESC index should be evaluated at various spatial scales and compared with existing maps of ecosystems; specifically, in catchments where multiple ESs are already mapped.

Indeed, we want to encourage PCA application in further studies, considering its feasibility and implications at larger scales (e.g. regional, national, etc.), while comparing this procedure with existing methods.

4.4. Discussion

The green network system obtained from PCA post-processing includes several key ecological areas, crossing the dense anthropic system that occupies the plain diffusely. It is noticeable how the anthropic system fragments Val Susa's natural ecosystem on the western side and the Turin hills and Monferrato from the easter. It is agreed that Urban Green multifunctional Networks should be capable of providing links between the primary ecological protected areas, while guaranteeing the continuity and contiguity of green multifunctional elements also in the dense built-up system (Liu et al., 2020). Therefore, the resulting PCA green network should be considered to restore an eco-systemically compatible urban connection between the Turin conurbation parks.

The Green network includes all the riverine areas, which become the ecological connection between the numerous natural areas that are included in the project "Corona Verde". The physical-environmental configuration of the green network can be summarized by identifying three distinct "core" ecological areas that are connected through few urban green elements (see Fig. 8), namely:

- the Alpine mountain system, placed on the west side of the city and constitutes the habitat refuge of various animal and plant species which find suitable living conditions;
- the hillside zone, at the east of Turin, which represents an ecological insula of naturalness that still maintains characteristics of relative homeostasis, surrounded by the densely urbanized plain;
- the densely inhabited plain, which stands between the Alpine and the hillside system, limits the natural exchanges between the two,

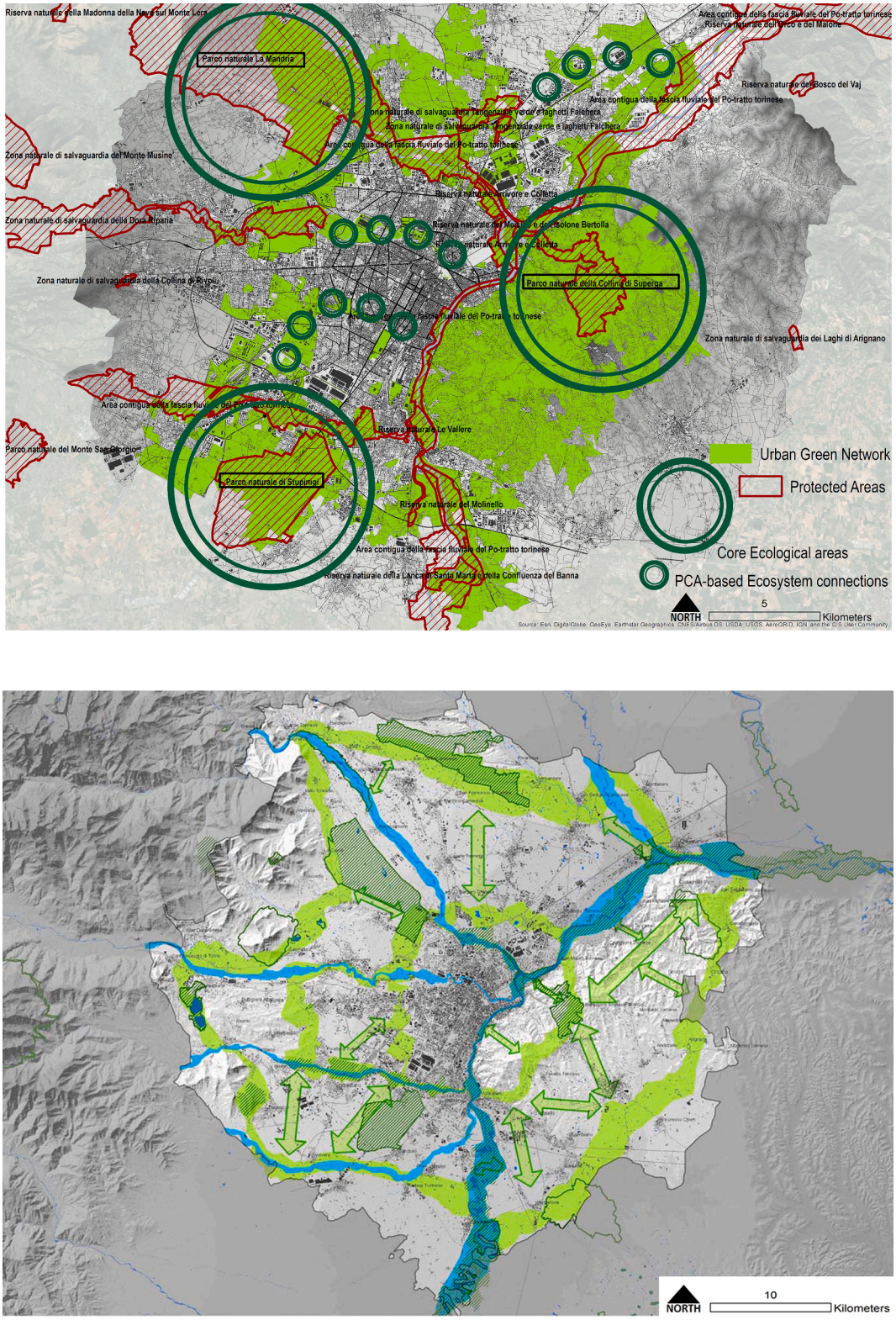

Fig. 8. Above: automatic PCA post-processing treatment to design the urban green network. Below: the Planned Metropolitan Green Belt of Turin, namely "Corona Verde - Masterplan, 2012". Source: Regione Piemonte (Copyright permission obtained). (For interpretation of the references to color in this figure legend, the reader is referred to the web version of this article.)

mainly for the Turin conurbation.

The city constitutes an ecological barrier between the Alpine system and the eastern hills, maintaining a high degree of naturalness and host natural functions. Further, the plain between north and south is heavily anthropized, but an agroecosystem with intensive farming is present. Here, the ecosystemic functioning is confined to narrow strips along with linear corridors between the urban environment and the wild protected zones such as the Regional Parks (see the core ecological areas in Fig. 8).

At a lower scale, one can identify at least three regional Protected

Areas that are included in the network: the Parco della Collina di Superga (est), Parco di Stupinigi (south-west) and Parco La Mandria (north-west).

The Parco della Collina di Superga is part of a hilly relief system, whose morphological variety and position, halfway between the Alps and the sea, ensure that micro-thermal species of alpine origin, alternating with the Mediterranean. The most common forest populations are mixed broad-leaved woods that were widely cultivated for timber and fruit production until a few decades ago.

Regarding Stupinigi, the site's ecological interest is due to the extensive forest area that has remained intact over time. In the forest, there are many species protected by the Habitat Directive, such as the plain queco-hornbeam, some strips of black alder wood (Alnus glutinosa) which are located in humid areas and locally enriched by the presence of a rare and peculiar species such as the cluster cherry (Prunus padus).

Finally, La Mandria is composed of a broad-leaved forest dominated by oaks, mainly Farnia, and common hornbeam. This lowland ecological system is an example of the widespread forest that occupied the European landscape in the ancient period, conserved as a hunting reserve during the XIX Century. La Mandria is a particular kind of ecological core metropolitan green area since it is a Communitarian protection zone (SIC) with a historical leisure/fruition function (inside the park there is still a Golf Course and a Motor Track of Fiat Chrysler Automobiles).

The connectivity among these three core areas is depicted by green corridors where the multifunctional ES delivering capacity is identified. Fig. 9 shows the potential connection between West-Est core ecological areas through a narrow strip connection along the Dora River and its neighbourhood adjacent green spaces (e.g. Parco della Pellerina, Parco Dora, Aurora district, Giardini Reali, New Campus Einaudi and Vanchiglietta district).

Inside the zone, there are some sports facilities, such as a swimming pool, soccer fields, a freely accessible skating rink, a BMX track in clay, bowls and tennis courts; however, some recently urban transformation areas are included (Campus Luigi Einaudi) as well as ancient gardens that border the Roman Castrum of the city. The inhabitants of Turin widely use these areas as places for walks, jogging, and leisure/recreational activities. Even if this green internal connection is enclosed in the dense settlement system, the co-presence of a multifunctional ecosystemic character is demonstrated by the presence of an aquatic fauna represented by various families of mallards, coots, moorhens and swans.

5. Conclusion

We have empirically tested the PCA method's employment as a numerical procedure for composite Ecosystem evaluation in this work. We have shown that the construction of a synthetic indicator on Ecosystem Service Capacity using the first component (PCA1) has several geostatistical benefits when used to define an Urban Green Network:

- The PCA1 indicator is more "clear", as it deletes more effectively the background "noise" of the simple Mean of GIS (see Fig. 4);
- It is also more "contrasted" as it generates a clearer distinction between high/low values of the composite Ecosystemic indicator (see Fig. 6);
- Finally, the PCA1 capacity is more consistent with representing the actual ESC status in the analysed catchment area (see Fig. 8).

These results follow the PCA's statistical properties, which resumes all the information content of the data; in particular, the spatial correlation between the input layers. This allows the subsequent GIS post-processing modelling to be more effective. Our empirical application to the Green Network design of the Turin area shows that PCA-based results are more consistent with existing hypotheses of planning built on local ground reliefs and analogic maps.

In general, the potential benefit of using the integrated PCA-based approach in building supervised environmental maps can be summarized as follows:

Fig. 9. The connectivity in the urban catchment. An example of how PCA post-processed network connects Parco della Pellerina (1), Parco Dora (2), Aurora (3), Giardini Reali (4), New Campus Einaudi (5), Vanchiglietta (6).

1. the basic PCA processing is nearly automatic and summarizes the information content of the data in such a way that each input component has specific weight;
2. it helps to detect also potential urban areas where multifunctional ES capacity must be delivered simultaneously;
3. it supports and increments the decision-making phase of land use planning by catching the "intrinsic character" of the Green Network;

In general, the PCA method becomes nearly mandatory when the number of input layers is high, as it always works as a dimensional reduction solution. Nonetheless, the PCA estimates cannot be worse than standard GIS overlying as the weighted Mean encompasses the simple one, with uniform weights. This brings benefits in at least three research areas: achieving higher quality and comprehension of the ESC gradients at the urban level, understanding the concentration of higher/lower clusters of multiple ecosystems, and supporting the decision-making process with sustainable green network design.

CRediT authorship contribution statement

Stefano Salata: Conceptualization, Investigation, Methodology, Supervision, Writing - original draft, Writing - review & editing. **Carlo Grillenzoni:** Conceptualization, Formal analysis, Investigation, Methodology, Software, Supervision, Validation, Writing - original draft, Writing - review & editing.

Declaration of Competing Interest

The authors declare that they have no known competing financial interests or personal relationships that could have appeared to influence the work reported in this paper.

Appendix A. Supplementary data

Supplementary data to this article can be found online at https://doi.org/10.1016/j.ecolind.2021.107758.

References

Alam, M., Dupras, J., Messier, C., 2016. A framework towards a composite indicator for urban ecosystem services. Ecol. Indic. https://doi.org/10.1016/j.ecolind.2015.05.035.

Arcidiacono, A., Ronchi, S., Salata, S., 2016. Managing Multiple Ecosystem Services for Landscape Conservation: A Green Infrastructure in Lombardy Region. In: Procedia Engineering. https://doi.org/10.1016/j.proeng.2016.08.831.

Baró, F., Palomo, I., Zulian, G., Vizcaino, P., Haase, D., Gómez-Baggethun, E., 2016. Mapping ecosystem service capacity, flow and demand for landscape and urban planning: A case study in the Barcelona metropolitan region. Land Use Policy 57, 405–417. https://doi.org/10.1016/j.landusepol.2016.06.006.

BenDor, T.K., Spurlock, D., Woodruff, S.C., Olander, L., 2017. A research agenda for ecosystem services in American environmental and land use planning. Cities 60, 260–271. https://doi.org/10.1016/j.cities.2016.09.006.

Borgogno-Mondino, E., Fabietti, G., Ajmone-Marsan, F., 2015. Soil quality and landscape metrics as driving factors in a multi-criteria GIS procedure for peri-urban land use planning. Urban For. Urban Green. 14, 743–750. https://doi.org/10.1016/j.ufug.2015.07.004.

Brenner, N., 2002. Decoding the Newest "Metropolitan Regionalism" in the USA: A Critical Overview. Cities 19, 3–21. https://doi.org/10.1016/S0264-2751(01)00042-7.

Brenner, N., Schmid, C., 2015. Towards a new epistemology of the urban? City 19, 151–182. https://doi.org/10.1080/13604813.2015.1014712.

Brunetta, G., Salata, S., 2019. Mapping Urban Resilience for Spatial Planning—A First Attempt to Measure the Vulnerability of the System. Sustainability 11, 1–24. https://doi.org/10.3390/su11082331.

Burkhard, B., Kroll, F., Nedkov, S., Müller, F., 2012. Mapping ecosystem service supply, demand and budgets. Ecol. Ind. 21, 17–29. https://doi.org/10.1016/j.ecolind.2011.06.019.

Burkhard, B., Crossman, N., Nedkov, S., Petz, K., Alkemade, R., 2013. Mapping and modelling ecosystem services for science, policy and practice. Ecosyst. Serv. 4, 1–3. https://doi.org/10.1016/j.ecoser.2013.04.005.

Caldarice, O., Salata, S., 2019. Valutare i Servizi Ecosistemici nel Piano come Risposta alla Vulnerabilità Territoriale. In: Una Riflessione Metodologica a partire dalla Proposta di Legge sul Consumo di Suolo in Piemonte | Ecosystem Service Assessment in Land Use Planning Decreasing Territo. Valori e Valutazioni, pp. 67–83.

Cassatella, C., 2013. The 'Corona Verde' Strategic Plan: an integrated vision for protecting and enhancing the natural and cultural heritage. Urban Res. Pract. 6, 219–228. https://doi.org/10.1080/17535069.2013.810933.

Crossman, N.D., Burkhard, B., Nedkov, S., Willemen, L., Petz, K., Palomo, I., Drakou, E. G., Martín-Lopez, B., McPhearson, T., Boyanova, K., Alkemade, R., Egoh, B., Dunbar, M.B., Maes, J., 2013. A blueprint for mapping and modelling ecosystem services. Ecosyst. Serv. 4, 4–14. https://doi.org/10.1016/j.ecoser.2013.02.001.

Dizdaroglu, D., Yigitcanlar, T., 2016. Integrating urban ecosystem sustainability assessment into policy-making: insights from the Gold Coast City. J. Environ. Plan. Manage. 59, 1982–2006. https://doi.org/10.1080/09640568.2015.1103211.

Faisal, K., Shaker, A., 2017. An investigation of GIS overlay and PCA techniques for urban environmental quality assessment: A case study in Toronto, Ontario, Canada. Sustain. 9, 1–25. https://doi.org/10.3390/su9030380.

Gavrilidis, A.A., Niţă, M.R., Onose, D.A., Badiu, D.L., Năstase, I.I., 2017. Methodological framework for urban sprawl control through sustainable planning of urban green infrastructure. Ecol. Indic. https://doi.org/10.1016/j.ecolind.2017.10.054.

Giaimo, C., Barbieri, C.A., Salata, S., 2019a. Ecosystem Services Based Approach for Participatory Spatial Planning and Risk Management in a Multi-Level Governance System. In: Urban Resilience for Risk and Adaptation Governance. Theory and Practice. Springer, Chan, pp. 59–74. https://doi.org/10.1007/978-3-319-76944-8_5.

Giaimo, C., Santolini, R., Salata, S., 2019b. Performace urbane e servizi ecosistemici. Verso nuovi standard?, in: Dopo 50 Anni Di Standard Urbanistici in Italia. Verso Percorsi Di Riforma. INU Edizioni, ROMA - ITA, pp. 63–69.

Giaimo, C., Salata, S., 2019. Ecosystem Services Assessment Methods for Integrated Processes of Urban Planning. The Experience of LIFE SAM4CP Towards Sustainable and Smart Communities. IOP Conf. Ser. Earth. Environ. Sci. 290, 012116 https://doi.org/10.1088/1755-1315/290/1/012116.

Graziano, P., Rizzi, P., 2016. Science of the Total Environment Vulnerability and resilience in the local systems : The case of Italian provinces. Sci. Total Environ. 553, 211–222. https://doi.org/10.1016/j.scitotenv.2016.02.051.

Grêt-Regamey, A., Weibel, B., Kienast, F., Rabe, S.-E., Zulian, G., 2015. A tiered approach for mapping ecosystem services. Ecosyst. Serv. 13, 16–27. https://doi.org/10.1016/j.ecoser.2014.10.008.

Grêt-Regamey, A., Altwegg, J., Sirén, E.A., van Strien, M.J., Weibel, B., 2017. Integrating ecosystem services into spatial planning—A spatial decision support tool. Landsc. Urban Plan. 165, 206–219. https://doi.org/10.1016/j.landurbplan.2016.05.003.

Grillenzoni, C., 2004. Adaptive spatio-temporal models for satellite ecological data. J. Agric. Biol. Environ. Stat. 9, 158–180. https://doi.org/10.1198/1085711043541.

Grillenzoni, C., 2008a. Statistics for image sharpening. Stat. Neerl. 62, 173–192. https://doi.org/10.1111/j.1467-9574.2007.00374.x.

Grillenzoni, C., 2008b. Design of kernel M-smoothers for spatial data. Stat. Methodol. 5, 220–237. https://doi.org/10.1016/j.stamet.2007.08.003.

Grillenzoni, C., 2016. Design of Blurring Mean-Shift Algorithms for Data Classification. J. Classif. 33, 262–281. https://doi.org/10.1007/s00357-016-9205-7.

Hansen, R., Olafsson, A.S., van der Jagt, A.P.N., Rall, E., Pauleit, S., 2019. Planning multifunctional green infrastructure for compact cities: What is the state of practice? Ecol. Ind. 96, 99–110. https://doi.org/10.1016/j.ecolind.2017.09.042.

Langemeyer, J., Gómez-Baggethun, E., Haase, D., Scheuer, S., Elmqvist, T., 2016. Bridging the gap between ecosystem service assessments and land-use planning through Multi-Criteria Decision Analysis (MCDA). Environ. Sci. Policy. https://doi.org/10.1016/j.envsci.2016.02.013.

Liu, Z., Xiu, C., Ye, C., 2020. Improving Urban Resilience through Green Infrastructure: An Integrated Approach for Connectivity Conservation in the Central City of Shenyang, China. In: Complexity 2020. https://doi.org/10.1155/2020/1653493.

Lovell, S.T., Taylor, J.R., 2013. Supplying urban ecosystem services through multifunctional green infrastructure in the United States. Landsc. Ecol. 28, 1447–1463. https://doi.org/10.1007/s10980-013-9912-y.

Maes, J., Liquete, C., Teller, A., Erhard, M., Paracchini, M.L., Barredo, J.I., Grizzetti, B., Cardoso, A., Somma, F., Petersen, J.E., Meiner, A., Gelabert, E.R., Zal, N., Kristensen, P., Bastrup-Birk, A., Biala, K., Piroddi, C., Egoh, B., Degeorges, P., Fiorina, C., Santos-Martín, F., Naruševičius, V., Verboven, J., Pereira, H.M., Bengtsson, J., Gocheva, K., Marta-Pedroso, C., Snäll, T., Estreguil, C., San-Miguel-Ayanz, J., Pérez-Soba, M., Grêt-Regamey, A., Lillebø, A.I., Malak, D.A., Condé, S., Moen, J., Czúcz, B., Drakou, E.G., Zulian, G., Lavalle, C., 2016. An indicator framework for assessing ecosystem services in support of the EU Biodiversity Strategy to 2020. Ecosyst. Serv. 17, 14–23. https://doi.org/10.1016/j.ecoser.2015.10.023.

McHarg, I.L., 1969. Design with nature, 25 anniver. ed. Wiley.

Mubareka, S., Koomen, E., Estreguil, C., Lavalle, C., 2011. Development of a composite index of urban compactness for land use modelling applications. Landsc. Urban Plan. 103, 303–317. https://doi.org/10.1016/j.landurbplan.2011.08.012.

Nin, M., Soutullo, A., Rodríguez-Gallego, L., Di Minin, E., 2016. Ecosystem services-based land planning for environmental impact avoidance. Ecosyst. Serv. 17, 172–184. https://doi.org/10.1016/j.ecoser.2015.12.009.

Palomo, I., Martín-López, B., Zorrilla-Miras, P., García Del Amo, D., Montes, C., 2013. Deliberative mapping of ecosystem services within and around Doñana National Park (SW Spain) in relation to land use change. Reg. Environ. Chang. 14, 237–251. https://doi.org/10.1007/s10113-013-0488-5.

Peccol, E., Movia, A., 2012. Evaluating land consumption and soil functions to inform spatial planning. In: 3rd International Conference on Degrowth for Ecological Sustainability and Social Equity. Venice, Italy, pp. 1–11.

Pulighe, G., Fava, F., Lupia, F., 2016. Insights and opportunities from mapping ecosystem services of urban green spaces and potentials in planning. Ecosyst. Serv. 22, 1–10. https://doi.org/10.1016/j.ecoser.2016.09.004.

Raymond, C.M., Frantzeskaki, N., Kabisch, N., Berry, P., Breil, M., Nita, M.R., Geneletti, D., Calfapietra, C., 2017. A framework for assessing and implementing the

co-benefits of nature-based solutions in urban areas. Environ. Sci. Policy 77, 15–24. https://doi.org/10.1016/J.ENVSCI.2017.07.008.
Rodarmel, C., Shan, J., 2002. Principal component analysis for hyperspectral image classification. Surv. L. Inf. Sci. 62, 115–122.
Rosenthal, A., Verutes, G., McKenzie, E., Arkema, K.K., Bhagabati, N., Bremer, L.L., Olwero, N., Vogl, A.L., 2015. Process matters: A framework for conducting decision-relevant assessments of ecosystem services. Int. J. Biodivers. Sci. Ecosyst. Serv. Manag. 11, 190–204. https://doi.org/10.1080/21513732.2014.966149.
Salata, S., 2019. Ecologically-Compatible Urban Planning: Designing a Healthier Environment, first ed. Emerald Publishing Limited, Howard House, Wagon Lane, Bingley BD16 1WA, UK.
Salata, S., Garnero, G., Barbieri, C., Giaimo, C., 2017. The Integration of Ecosystem Services in Planning: An Evaluation of the Nutrient Retention Model Using InVEST Software. Land 6, 1–21. https://doi.org/10.3390/land6030048.
Salata, S., Giaimo, C., Barbieri, C.A., Garnero, G., 2019. The utilization of ecosystem services mapping in land use planning: the experience of LIFE SAM4CP project. J. Environ. Plan. Manage. https://doi.org/10.1080/09640568.2019.1598341.
Schröter, M., Remme, R.P., Sumarga, E., Barton, D.N., Hein, L., 2015. Lessons learned for spatial modelling of ecosystem services in support of ecosystem accounting. Ecosyst. Serv. 13, 64–69. https://doi.org/10.1016/j.ecoser.2014.07.003.
Sharps, K., Masante, D., Thomas, A., Jackson, B., Redhead, J., May, L., Prosser, H., Cosby, B., Emmett, B., Jones, L., 2017. Comparing strengths and weaknesses of three ecosystem services modelling tools in a diverse UK river catchment. Sci. Total Environ. 584, 118–130. https://doi.org/10.1016/j.scitotenv.2016.12.160.
Smith, A.C., Harrison, P.A., Pérez Soba, M., Archaux, F., Blicharska, M., Egoh, B.N., Erős, T., Fabrega Domenech, N., György, I., Haines-Young, R., Li, S., Lommelen, E., Meiresonne, L., Miguel Ayala, L., Mononen, L., Simpson, G., Stange, E., Turkelboom, F., Uiterwijk, M., Veerkamp, C.J., Wyllie de Echeverria, V., 2017. How natural capital delivers ecosystem services: A typology derived from a systematic review. Ecosyst. Serv. 26, 111–126. https://doi.org/10.1016/j.ecoser.2017.06.006.
Switzer, P., Green, A.A., 1984. Min/Max Autocorrelation factors for multivariate spatial imagery. Technical Report No. 6. Stanford, California.
Tabachnick, B.G., Fidell, L.S., 2013. Using Multivariate Statistics, 6th ed. Pearson.
Tallis, H.T., Ricketts, T., Guerry, A.D., Wood, S.A., Sharp, R., Nelson, E., Ennaanay, D., Wolny, S., Olwero, N., Vigerstol, K., Pennington, D., Mendoza, G., Aukema, J., Foster, J., Forrest, J., Cameron, D., Arkema, K., Lonsdorf, E., Kennedy, C., Verutes, G., Kim, C.K., Guannel, G., Papenfus, M., Toft, J., Marsik, M., Bernhardt, J., 2011. InVEST 2.0 beta User's Guide, The Natural Capital Project. Stanford.
Turkelboom, F., Thoonen, M., Jacobs, S., Berry, P., 2015. Ecosystem Service Trade-offs and Synergies. Ecol. Soc. 21 (43) https://doi.org/10.13140/RG.2.1.4882.9529.
Van der Meulen, S., Linda Maring, L., Bartkowski, B., Hagemann, N., Arrúe, J.L., Playán, E., Castañeda, C., Herrero, J., Plaza, D., Álvaro-Fuentes, J., Sànchez, F.M., Lopatka, A., Siebielec, G., Verboven, J., De Cleen, M., Staes, J., Boekhold, S., Goidts, E., Salomez, J., Creamer, R., Alberico, S., Abdul Malak, D., Soraci, M., Munafo, M., Bal, N., Baritz, R., Molenaar, C., Brils, J., Akzoy, E., Baritz, R., Cousin, I., Hessel, R., Dejonckheere, A., Bartke, S., Salata, S., Marin, A., Verzandvoort, S., Jones, A., Maes, J., Vallecillo, S., De Angelis, A., Innamorati, A., Orgiazzi, A., Bertaglia, M., Teller, A., Forlin, V., Masson, J., Delsalle, J., Olazabal, C., Peeters, B., 2018. Mapping and Assessment of Ecosystems and their Services; Soil ecosystems.
Voghera, A., Giudice, B., 2019. Evaluating and planning green infrastructure: A strategic perspective for sustainability and resilience. Sustain. 11 https://doi.org/10.3390/su11102726.
Young, R.F., McPherson, E.G., 2013. Governing metropolitan green infrastructure in the United States. Landsc. Urban Plan. 109, 67–75. https://doi.org/10.1016/j.landurbplan.2012.09.004.
Zardo, L., Geneletti, D., Pérez-soba, M., Eupen, Van, M., 2017. Estimating the cooling capacity of green infrastructures to support urban planning. Ecosyst. Serv. 26, 225–235. https://doi.org/10.1016/j.ecoser.2017.06.016.